Chemical-looping combustion with heavy liquid fuels in a 10 kW pilot plant

Chemical-Looping Combustion with Heavy Liquid Fuels in a 10 kW Pilot Plant

Patrick Moldenhauer[a,*], Magnus Rydén[a], Tobias Mattisson[a], Aqil Jamal[b], Anders Lyngfelt[a]

[a] *Chalmers University of Technology, Department of Energy and Environment, 412 96 Gothenburg, Sweden*
[b] *Saudi Aramco, Research & Development Center, 313 11 Dharan, Kingdom of Saudi Arabia*

Abstract

In this study, chemical-looping combustion was performed with highly viscous vacuum residue. A fuel reactor with a fuel-injection system for liquid fuels was designed and built for a chemical-looping reactor with the nominal fuel input of 10 kW_{th}. The gas velocities in the riser section and at the gas-distribution nozzles of this unit are comparable to those of industrial circulating fluidized-bed boilers. Reference experiments were performed with an ilmenite oxygen carrier and two different fuel blends that contained 40 wt% and respectively 80 wt% of vacuum residue in fuel oil 1. Fuel conversion was in line with that of experiments from an earlier campaign, where fuel oil 1 was used as fuel. The fuel contained a significant fraction of sulfur, but no SO_2 was detected in the flue gas of the air reactor.

More experiments were performed using an oxygen carrier based on calcium manganite. The oxygen carrier was exposed to fluidization at hot conditions (more than 600°C) for about 95 h, out of which fuel was injected during a total of 9.6 h. Undiluted vacuum residue, fuel oil 1 as well as different blends of these two were used as fuel. Furthermore, the parameters fuel flow, fuel-reactor temperature and air flow in the air reactor were varied to observe trends in fuel conversion. The experiments were carried out with a fuel flow corresponding to 4.0–6.2 kW_{th} and an oxygen carrier-to-fuel ratio of about 1300–2000 kg/MW_{th} (fuel-reactor bed mass per thermal fuel-power). With undiluted vacuum residue as fuel and a fuel-reactor temperature of 1000°C, up to 93% of all carbon leaving the fuel reactor was in the form of CO_2. Carbon leakage from fuel reactor to air reactor was usually below 1% for all fuel types tested, but no SO_2 was detected in the off-gas from the air reactor. The reactivity of the calcium manganite-based material decreased over the course of the experiments, which is likely due to sulfur poisoning. No defluidization or agglomeration problems were experienced over the course of the experimental campaign.

Keywords: chemical-looping combustion (CLC), liquid fuel, vacuum residue, calcium manganite, ilmenite, CO_2 capture, carbon capture and storage (CCS)

1. Introduction

1.1. Chemical-Looping Combustion

Chemical-looping combustion (CLC) is a method of using carbon-based fuels for production of heat with inherent separation of CO_2. CLC can be part of a CCS (carbon capture and storage) scheme with the purpose of reducing the impact of carbon dioxide from carbon-based fuels on the climate of the Earth. Continued utilization of fossil fuels at a large scale will require implementation of CCS if the UN and EU endorsed temperature limits are to be met [1, 2].

In chemical-looping combustion an active bed material, the oxygen carrier, is cyclically exposed to oxidizing and reducing atmospheres, respectively air and fuel. While in air, the oxygen carrier takes up oxygen and subsequently passes it to the fuel. This can be achieved by circulating the oxygen-carrier particles continuously between two fluidized-bed reactors. The net reaction of this process is the same as for combustion in air, i.e., the heat produced in chemical-looping combustion is the same as in combustion in air. The difference is that in chemical-looping combustion the fuel is never mixed with nitrogen from the air, so that the off-gas from the fuel reactor ideally consists of only carbon dioxide and steam. The latter can be condensed and the sequestration of CO_2 does not require any input of energy. Recent literature concerning developments, advancements and operational experience in different chemical-looping applications has been published by Adánez et al. [3], Lyngfelt [4] and Nandy et al. [5].

1.2. Liquid Fuels in Chemical-Looping Combustion

The use of liquid fuel in stationary combustion processes is far less common than the use of coal or gas. Because of their high energy density, liquid fuels are mostly used in transport applications. In an oil refining process, a large variety of end products can be generated, which differ greatly in quality and price. The bottom residues of a vacuum distillation process, also called vacuum residues, are upgraded if economically feasible. Such low-grade heavy-oil products could pose an interesting and feasible option for thermal processes, especially if the process is located close to or integrated in a refinery process, where there is a constant need for heat and steam. Difficulties in the use of heavy-oil products are related to their high viscosity and

*Corresponding author. *Telephone:* +46 (0)31-772 1469
E-mail address: patrick.moldenhauer@chalmers.se (Patrick Moldenhauer)

to high amounts of sulfur and other impurities, such as heavy metals. A recent overview about chemical-looping combustion of liquid fuels has been published by Rydén [6].

2. Experimental Details

2.1. 10 kW Chemical-Looping Combustion Reactor System

Figure 1 shows a schematic of the reactor system with all major sections shown, including gas and fuel inlets and gas exits. The unit is based on interconnected fluidized beds and is similar to the design originally presented by Lyngfelt et al. [7]. In the riser section there is a fast-fluidized regime, whereas in the loop-seals and the fuel reactor there is a bubbling regime. In the air reactor the fluidization regime is on the transition between bubbling and fast fluidized. The unit was heated externally to maintain sufficient temperature in the system and compensate for radiation losses. Such losses are inherent in small-scale units like the one used here, i.e., such with a high ratio of surface area to volume. Additionally, the air that is fed to the air reactor is preheated to 1000°C. The heating cables are wrapped around the riser section, the cyclone, the upper loop-seal and the fuel reactor, and covered with insulation material. More details about the reactor system can be found elsewhere [8].

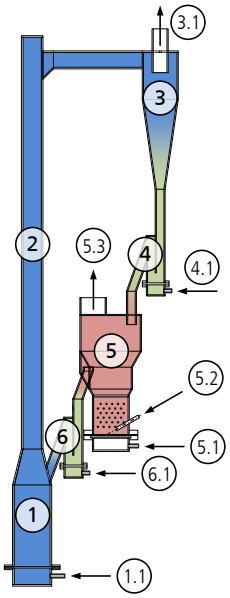

1 – air reactor (ID 150 mm)
1.1 – air-reactor fluidization (air)
2 – riser (ID 80 mm, H_{tot} 2.2 m)
3 – cyclone
3.1 – air-reactor gas outlet
4 – upper loop-seal
4.1 – loop-seal fluidization (nitrogen)
5 – fuel reactor (ID 150→260 mm)
5.1 – fuel-reactor fluidization (steam/nitrogen)
5.2 – fuel inlet (fuel/steam)
5.3 – fuel-reactor gas outlet
6 – lower loop-seal
6.1 – loop-seal fluidization (nitrogen)

Figure 1: Schematic of the 10 kW chemical-looping combustion reactor

The lower section of the fuel reactor was specifically designed for direct injection of liquid fuel, see Figure 2. The height of this section is about 165 mm and the bed diameter is 150 mm. The total bed height in the fuel reactor is 275 mm. Steam is used to fluidize the oxygen-carrier particles at a superficial gas velocity that corresponds to about 7–20 times the minimum fluidization velocity, u_{mf}. Fuel is introduced via an exchangeable injection nozzle with an orifice diameter of 0.25 mm. The injection nozzle and the fuel jet are surrounded by a flow of steam, which has the purpose of cooling injection system and fuel jet as well as preventing oxygen-carrier particles from entering the injection system. To reduce heat transfer from the hot particle bed to the injection system, the injection nozzle is located as far away as possible from the bed, while being as close as necessary for the fuel jet to reach the bed. In the fluidized bed reactor, 31 rods with a diameter of 6 mm are arranged in an equidistant pattern, which are referred to as internals. These internals are used to limit the growth of gas bubbles and to reduce the risk of formation of gas channels, which would reduce the fuel–oxygen carrier contact and therefore decrease fuel conversion. The projected open area that results from the pattern of the internals corresponds to 54% of the total cross-sectional area of the fuel reactor. A plate with 55 holes, which have a diameter of 0.5 mm an are arranged in an equidistant pattern, acts as gas distributor in the bottom of the fuel reactor. The porous quartz, which is located below the hole plate, was intended to be used as gas distributor in an earlier design phase, but became redundant when the hole plate was introduced.

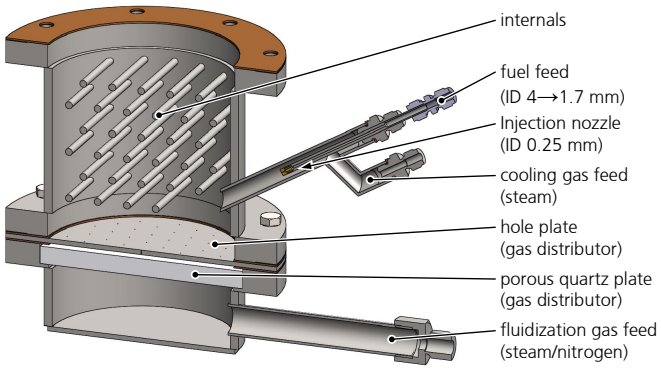

Figure 2: Lower section of the fuel reactor for direct injection of liquid fuel. During operation, this section is completely filled with fluidized oxygen-carrier particles.

The amount of oxygen carrier used in the 10 kW unit depends on the bulk density of the oxygen-carrier particles. In the configuration used for injection of liquid fuel, the bed mass is in the range of 15–25 kg, out of which 5–10 kg are in the fuel reactor.

2.2. Measurements

During the experiments, measurements of pressure, temperature, gas flows and gas concentrations are logged continuously. The fuel flow is logged manually and is based on the measured weight of the fuel tank. A schematic description of the system for gas analysis is shown in Figure 3.

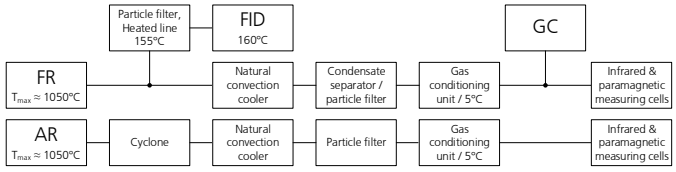

Figure 3: Schematic description of the gas-analysis system

Small streams of the flue gases from air reactor (AR) and fuel reactor (FR), ca. 1 L_n/min on a dry basis, are diverted from

the main gas streams, filtered, cooled to about 4°C and fed to gas analyzers. Gas concentrations of O_2 (paramagnetic sensor) and CO, CO_2 and CH_4 (infrared sensors) are measured continuously in the flue gases from both reactor vessels.

A fraction of the dried gas stream of the fuel reactor is fed to a micro gas-chromatograph (GC) with two parallel columns (Molsieve MS5Å, 10 m × 0.32 mm and PoraPLOT Q, 10 m × 0.15 mm), which both are equipped with a thermal-conductivity detector. In the gas chromatograph, concentrations of H_2, N_2, O_2, CO, CH_4, CO_2, C_2H_n and C_3H_n[1] are detected and quantified. Another small stream of the fuel reactor gases is kept above 155°C and analyzed separately and continuously in a flame-ionization detector (FID), which measures the total carbon content in organic compounds, i.e., approximately $\sum\left(x \cdot C_xH_yO_z\right)$.

SO_2 in the flue gases of the air reactor was measured on a few occasions by means of an infrared sensor. On one occasion, with ilmenite oxygen carrier, H_2S and SO_2 were measured intermittently in the flue gases of the fuel reactor using detector tubes (Dräger), which give a colorimetrical indication of the dry-gas concentration for specific gas species. For the specific detector tubes used here, the lower detection limits are 50 ppm and 2000 ppm for SO_2 and H_2S, respectively. It should be mentioned that the measurement system for the fuel reactor, where there are substantial amounts of steam and condensate, was not specifically adapted for measuring SO_2, which has a high solubility in water.

2.3. Oxygen-Carrier Materials

2.3.1. Ilmenite

Ilmenite is a mineral that is composed mainly of iron–titanium oxide ($FeTiO_3$) as well as some hematite (Fe_2O_3). Before mineral ilmenite can be used as a bed material in a chemical-looping process, it is ground, physically beneficiated and calcined.

The ilmenite oxygen carrier used here was a mixture of about 75 wt% particles used during a previous campaign with fuel oil 1 as fuel and 25 wt% of fresh, uncalcined particles. The harmonic mean size on weight basis of the fresh material was 130 µm, but most likely increased during calcination and initial oxidation/reduction cycles. The used particles had a weight-based harmonic mean size of 160 µm. Details regarding the test campaign with fuel oil 1 as well as more information about ilmenite and its use in chemical-looping processes can be found elsewhere [9].

2.3.2. Calcium Manganite

A calcium manganite-based bed material with a perovskite structure was used that had a nominal composition $CaMn_{0.775}Ti_{0.125}Mg_{0.1}O_{3-\delta}$. The particles used had a harmonic mean size of 159 µm (x_{10} = 96 µm and x_{90} = 234 µm), based on weight, and were produced by VITO NV in Mol, Belgium, through spray-drying followed by calcination at 1350°C for 4 h. This oxygen carrier can release gas-phase oxygen in the fuel reactor, which is usually referred to as CLOU (chemical-looping with oxygen uncoupling). This allows for a direct reaction of fuel with gaseous oxygen, which is expected to improve the conversion of intermediate and heavy liquid fuels noticeably.

A similar oxygen-carrier material has been used during commissioning of the 10 kW reactor system with injection of fuel oil 1 and delivered promising results regarding fuel conversion [9]. Oxygen-carrier materials with the same nominal composition as the one used here, were used for tests in a batch fluidized-bed reactor with different gaseous fuels [10–13], as well as in 300 W, 10 kW and 120 kW circulating fluidized-bed reactors with a sulfur-free natural gas as fuel [10, 14, 15].

Calcium manganite-based materials are usually deactivated by sulfur. In the presence of either SO_2 or H_2S deactivation occurs, most likely a consequence of formation of CaS, $CaSO_3$ or $CaSO_4$. An experimental investigation showed that the specific material used here has a higher resistance to sulfur poisoning, as compared to similar materials that are not doped with Ti and Mg [11]. This investigation also demonstrated that regeneration of the oxygen carrier is possible during reduction in the absence of sulfur.

2.4. Fuels

The fuels used were based on a vacuum residue with about 5 wt% of sulfur. Straight vacuum residue was used as well as different blends with a diesel-type fuel oil 1 with low sulfur content.

2.4.1. Vacuum Residue

Vacuum residue is the bottom product of a vacuum distillation in an oil refinery process. Prior to vacuum distillation, crude oil is fractionated in a crude distillation unit, which operates at atmospheric pressure. The residue of the crude distillation unit is used as feedstock for a vacuum distillation unit, where the vacuum residue is obtained. Vacuum residue is an intermediate and low-value product that can be either converted to asphalt in an asphalt blower or upgraded in a delayed coking process to more valuable products, like naphtha or gas oils. The by-product from this upgrading process is petroleum coke. A comprehensible and illustrated summary of the different processes in an oil refinery was published by Olsen [16]. A comprehensive report on heavy fuel oils, which have many similarities with vacuum residue, was compiled by the American Bureau of Shipping [17].

The vacuum residue used here was provided by courtesy of Saudi Aramco, Kingdom of Saudi Arabia. Vacuum residue generally has a high viscosity, which makes handling difficult. Additionally, it contains contaminants, like sulfur and different heavy metals, which can cause corrosion or fouling problems. The viscosities of the vacuum residue, the fuel oil 1 and different blends of both are shown in Figure 4. A boiling range distribution of the vacuum residue, performed at reduced pressure, is shown Figure 5. As can be seen, vacuum residue cannot be fully distilled like lighter hydrocarbons because of initiation of thermal cracking, which leads to fouling. Further fuel properties can be found in Table 1.

[1] C_2H_n and C_3H_n are substitute denominations for hydrocarbons with two and three carbon atoms, respectively. This includes the species C_2H_2, C_2H_4 and C_2H_6 and C_3H_4, C_3H_6 and C_3H_8.

To reduce the viscosity of the vacuum residue and to make it flowable, it was preheated to 80°C in the fuel tank and in the fuel line when used without fuel oil as dilutant.

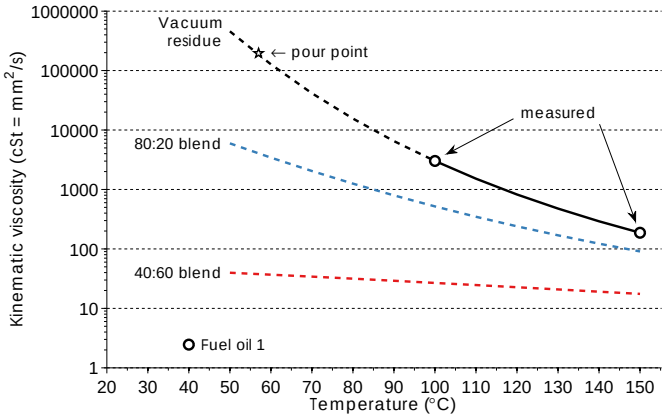

Figure 4: Kinematic viscosity at different temperatures of vacuum residue, fuel oil 1 and different blends of both. For vacuum residue, the pour point is shown.[2]

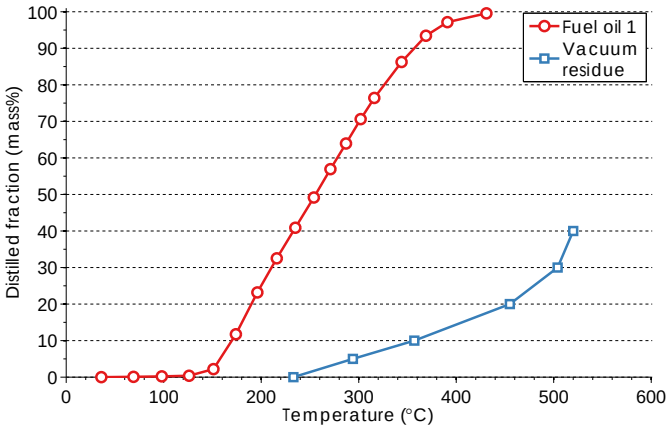

Figure 5: Boiling range distribution of fuel oil 1 and vacuum residue according to ASTM standards D 2887 and D 1160, respectively.

2.4.2. *Fuel Oil 1*

The fuel oil, which is usually used as domestic heating/fuel oil, has the commercial name Eo1 E10 and was purchased from a local provider, Preem AB in Gothenburg, Sweden. It meets the requirements for fuel oil defined in the Swedish standard SS 155410 [19]. An elemental analysis was performed and density and heating values were measured, see Table 1. Additionally, a distillation curve was determined according to ASTM standard D 2887, see Figure 5. The fuel contains about 15 vol% aromatic compounds.

[2]The viscosity of the vacuum residue and the fuel oil 1 were measured according to ASTM standards D 445 and ISO 3104, respectively. The kinematic viscosities of the blends of vacuum residue and fuel oil 1 were calculated according to Shu [18]. The pour point is defined as the lowest temperature at which, upon cooling, movement of a liquid is observed and was determined according to ASTM standard D 97.

2.4.3. *Blends of Fuel Oil and Vacuum Residue*

As can be seen in Figure 4, blending the vacuum residue with the fuel oil 1 causes a dramatic reduction in viscosity. Hence, little or no heating is necessary to handle and pump the fuel. Using cold fuel instead of preheated fuel can be an important contribution towards a reduction in fuel temperature in the fuel injector. Above a certain temperature, ca. 350°C, thermal decomposition followed by polymerization can occur in the fuel [20], which can lead to blocking of the injector.

Two different blends of vacuum residue and fuel oil were prepared and used as fuel: 40 wt% vacuum residue in fuel oil and 80 wt% vacuum residue in fuel oil (from here on referred to as 40:60 blend and 80:20 blend, respectively). The 40:60 blend did not require any preheating, whereas the 80:20 blend was preheated to 30°C in the fuel tank and kept at that temperature in the feeding system.

2.5. *Parameters Investigated*

2.5.1. *Ilmenite Oxygen carrier*

Tests with ilmenite oxygen carrier were performed using the 40:60 blend and the 80:20 blend. Experiments with fuel addition were conducted for a total of 3.9 h. The goal during this test campaign was to test the fuel-injection system and to establish reference values regarding the conversion of blends of vacuum residue and fuel oil. The experimental parameters used with ilmenite oxygen carrier can be found in Table 2.

2.5.2. *Calcium Manganite-based Oxygen Carrier*

The calcium manganite-based oxygen carrier was tested with fuel oil 1, 40:60 and 80:20 blends as well as undiluted vacuum residue for a total of 9.6 h of fuel addition. The goal of this campaign was to conduct tests with undiluted vacuum residue. The parameters used in this campaign are summarized in Table 2.

Reactivity Analysis. To assess whether the reactivity of an oxygen carrier changed over the course of the experiments, i.e., through activation or deactivation, several oxidation and reduction cycles were performed in a batch fluidized-bed reactor with both fresh and used oxygen carrier. Tests were performed using methane as fuel, as it was judged to give a good indication and basis of comparison for the oxygen transfer rate of the oxygen carrier. The fluidized-bed reactor is made of quartz glass and is 820 mm high. 370 mm from the bottom, a porous quartz plate is located, which has a diameter of 22 mm and acts as gas distributor for the fluidized bed. For the reactivity analysis, 6 g of the calcium manganite-based oxygen carrier were mixed with 9 g of quartz sand, both in the size fraction of 125–180 µm. During warm-up, the oxygen carrier was fluidized with 10% O_2 in N_2 to ensure that it was fully oxidized prior to the experiments. At 950°C, the oxygen carrier was then alternatingly reduced and oxidized to mimic chemical-looping redox cycles. Methane was used for 18 s during the reduction period and the experiment was repeated four times. In between oxidation and reduction cycles, the system was purged with nitrogen for 60 s to avoid the mixing of gases. The inlet flow-rate was 0.90 L_N/min during oxidation and inert periods and 0.86 L_N/min during reduction, which corresponds to a specific bed mass of 13 kg/MW_{th}.

Table 1: Results of the analyses on fuel oil 1 and vacuum residue

Analysis parameter	Unit	Fuel type		Analysis method
		Fuel oil 1	Vacuum residue	
Carbon content	mass%	86.6 ± 0.5	84.5 ± 0.5	ASTM D 5291
Hydrogen content	mass%	13.7 ± 0.4	10.3 ± 0.3	ASTM D 5291
Nitrogen content	mass%	<0.1 ± 0.03	0.4 ± 0.1	ASTM D 5291
Sulfur content	mg/kg	<500 ± 40	48100 ± 3100	ASTM D 1552
Ash content	mg/kg	<100	330 ± 60	ISO 6245 (FO1), ASTM D 482 (VR)
Vanadium content	mg/kg	not tested	121 ± 25	ASTM D 5185
Nickel content	mg/kg	not tested	35 ± 12	ASTM D 5185
Natrium content	mg/kg	not tested	19 ± 8.2	ASTM D 5185
Lower heating value	MJ/kg	43.00 ± 0.21	39.56 ± 0.19	ASTM D 240
Higher heating value	MJ/kg	45.91 ± 0.22	41.74 ± 0.20	ASTM D 240
Density	kg/dm^3	0.832 ± 0.001*	1.01†	see footnotes
Hydrogen-to-carbon ratio	mol/mol	1.89 ± 0.07	1.45 ± 0.07	calculated

FO1: fuel oil 1 VR: vacuum residue

*measured at 15°C in vacuum according to ASTM D 4052

†measured at 20°C at atmospheric pressure

Table 2: Experimental parameters during experimental campaigns with ilmenite and calcium manganite-based oxygen carriers

Experimental parameter	Unit	Value	
		Ilmenite	Calcium manganite
Superficial gas velocities			
Fuel reactor (steam)	(m/s)	0.11–0.14	0.12–0.15
Air reactor (air)	(m/s)	0.69–0.92	0.74–0.97
Riser (air)	(m/s)	2.5–3.2	2.6–3.4
Slip velocity in Riser $[(u_0 - u_t)/u_t]$	(–)	3.2–4.9	2.6–3.9
Air-to-fuel ratio*	(mol/mol)	2.1–2.8	1.8–3.1
Fuel reactor temperature	(°C)	830–960	950 and 1000
Fuels tested	n/a	80:20 & 40:60 blends†	Vacuum residue, 80:20 & 40:60 blends, fuel oil 1
Fuel flow	(ml_{liq}/min)	≈ 7.4–9.0	6.1–10.5
	(kW_{th})	≈ 4.6–5.6	4.0–6.2
Bed mass in fuel reactor	(kg)	≈ 7.7	≈ 8.1
	(kg/MW_{th})	≈ 1400–1700	≈ 1300–2000
Total bed mass	(kg)	≤ 22	16–21

*The air-to-fuel ratio is the molar ratio of air fed to the air reactor and the stoichiometric amount of air needed for complete combustion of fuel.

†A test campaign with ilmenite oxygen carrier and fuel oil 1 is the subject of an earlier publication by the authors [9].

3. Data Evaluation

3.1. Oxygen-Carrier Circulation

One way to quantify the circulation of solids in a circulating fluidized-bed (CFB) reactor is through the mass flux of solids, G_s, which expresses the circulation as mass flow per area in kg/m^{2}s. Normally, the cross-sectional area of the riser is used as reference. This allows for comparison of solid circulation of CFB units of different size. It is usually not possible to measure the mass flux of solids directly. Here, the mass flux of solids is calculated based on pressure-difference measurements that are extrapolated to obtain the bed density at the exit of the riser, ρ_{exit}, see Equation (1) [21].

$$G_s = \rho_{exit} \cdot (u_0 - u_t) = -\frac{1}{g} \cdot \frac{dp_{exit}}{dh_{exit}} \cdot (u_0 - u_t) \quad (1)$$

For practical reasons, Equation (1) is simplified and adapted to the 10 kW unit, see Equation (2). To make a clear distinction between the true mass flux of solids and the calculated value, G'_s, the latter is referred to as the circulation index, see Equation (2). The circulation index, which is based on a pressure-difference measurement in the middle of the riser, represents the gross amount of particles, i.e., the sum of particles traveling upward and downward and, consequently, gives an overestima-

tion of the true mass flux of solids, G_s. The circulation index is assumed to be proportional to the true mass flux.

$$G'_s = -\frac{1}{g} \cdot \frac{\Delta p}{\Delta h} \cdot (u_0 - u_t) \tag{2}$$

The terminal velocity, u_t, is approximated according to Kunii and Levenspiel [22].

3.2. Fuel Conversion

A simple and straightforward way to evaluate the conversion of fuel is to compare the amount of oxygen consumed in the air reactor with the stoichiometric amount of oxygen needed for full conversion of fuel to CO_2 and H_2O. Equation (3) shows how the degree of fuel oxidation, η_{fuel}, is calculated.

$$\eta_{fuel} = \frac{\dot{n}_{O_2,AR,in} - \dot{n}_{O_2,AR,out}}{\dot{n}_{O_2,stoich}} \tag{3}$$

The significance of Equation (3) strongly depends on the amount of fuel that leaks into the air reactor. If a large amount of fuel leaks into the air reactor, e.g., as coke or reactive gas, oxygen consumption will still be high but at a sacrifice of CO_2 capture efficiency. On the basis of the concentration of CO_2 in the exhaust gases from the air reactor, the fraction of fuel carbon that leaks into the air reactor, $f_{C,AR}$, is determined according to Equation (4). The flow of CO_2 leaving the air reactor is compensated for the atmospheric concentration of CO_2, which was approximately 400 ppm during the time of the experiments.

$$f_{C,AR} = \frac{\dot{n}_{CO_2,AR,out}}{\dot{n}_{C,fuel}} \tag{4}$$

Another way to evaluate the conversion of fuel, which gives more detailed information about the different steps of conversion and selectivity, is to quantify the different species in the exhaust gas of the fuel reactor. The measurement equipment used, cf. Section 2.2, allows for monitoring the fate of fuel carbon. The different carbon species are calculated according to Equations (5)–(8). The fraction of CO_2 of the total amount of carbon in the exhaust gases of the fuel reactor is called the CO_2 yield. A special denotation, γ instead of f, is chosen to differentiate CO_2 as desired oxidation product from other carbon species CO, CH_4 and $C_xH_yO_z$.

$$\gamma_{CO_2} = \frac{\dot{n}_{CO_2,FR}}{\dot{n}_{CO_2,FR} + \dot{n}_{CO,FR} + \sum\left(x \cdot \dot{n}_{C_xH_yO_z,FR}\right)} \tag{5}$$

$$f_{CO} = \frac{\dot{n}_{CO,FR}}{\dot{n}_{CO_2,FR} + \dot{n}_{CO,FR} + \sum\left(x \cdot \dot{n}_{C_xH_yO_z,FR}\right)} \tag{6}$$

$$f_{CH_4} = \frac{\dot{n}_{CH_4,FR}}{\dot{n}_{CO_2,FR} + \dot{n}_{CO,FR} + \sum\left(x \cdot \dot{n}_{C_xH_yO_z,FR}\right)} \tag{7}$$

$$f_{CHO} = \frac{\sum\left(x \cdot \dot{n}_{C_xH_yO_z,FR}\right) - \dot{n}_{CH_4,FR}}{\dot{n}_{CO_2,FR} + \dot{n}_{CO,FR} + \sum\left(x \cdot \dot{n}_{C_xH_yO_z,FR}\right)} \tag{8}$$

3.3. Oxygen-Carrier Reactivity in Batch Tests

For each cycle of the reactivity analysis, gas conversion and oxygen-carrier conversion are calculated. The oxygen-carrier conversion, i.e., the degree of mass-based conversion, ω, is calculated from the actual mass of the oxygen carrier, m_{OC}, and its mass in the most oxidized state, $m_{OC,ox}$, see Equation (9). The gas conversion, i.e., the gas yield of CO_2, γ_{CO_2}, is calculated for methane as fuel according to Equation (10) and is based on measured gas concentrations, x_i.

$$\omega = \frac{m_{OC}}{m_{OC,ox}} \tag{9}$$

$$\gamma_{CO_2} = \frac{x_{CO_2}}{x_{CO_2} + x_{CO} + x_{CH_4}} \tag{10}$$

4. Results

4.1. Ilmenite Oxygen Carrier

Figure 6 shows the degree of fuel oxidation, η_{fuel}, at varied circulation index, G'_s, fuel-reactor temperature and fuel type. As a reference, additional values are shown from experiments with ilmenite oxygen carrier and fuel oil 1 [9]. The flow rates of fuel for the reference points correspond to 3.9–4.5 kW_{th}. Even though the flow rates of air in the riser here were similar to those of the reference values, the circulation index was clearly lower. The operation temperature was limited to 950°C due to problems with the electrical heating cables.

When using blends of vacuum residue and fuel oil 1, the degree of fuel oxidation seems to improve at higher temperatures. A dependence on fuel type or circulation index cannot be clearly identified due to a low amount of data points as well as a high variation of results, which is probably a result of the short periods of stable operation. The concentration of oxygen measured at the outlet of the air reactor varied between 15.1% and 18.4% for the different experimental settings. The highest degree of fuel oxidation was just below 87% and was achieved with the 40:60 blend as fuel and at a temperature of 950°C. Generally, fuel conversion with blends of vacuum residue and fuel oil 1 was in line with that from the experiments where only fuel oil 1 was used as fuel. The differences in fuel conversion seen in Figure 6 could be explained by differences in solids circulation as well as unstable fuel feeding.

Carbon leakage to the air reactor, $f_{C,AR}$, was estimated based on measured concentrations of CO_2 in the air reactor, which were corrected for the atmospheric concentration of CO_2, i.e., 400 ppm. The highest amount of carbon leakage by far was 8.3% of the fuel carbon and was measured during the experiment with the highest degree of fuel oxidation, i.e., the fuel used was the 40:60 blend and the temperature was 950°C. Even though carbon leakage was highest for the largest value of the circulation index, a general dependence of carbon leakage on solids circulation is not observed. Carbon leakage during the rest of the experiments was between 0.4% and 2.5%.

During one test with the 80:20 blend as fuel, SO_2 was measured continuously for 16 min in the flue gas of the air reactor. Additionally, SO_2 and H_2S were measured once each in the

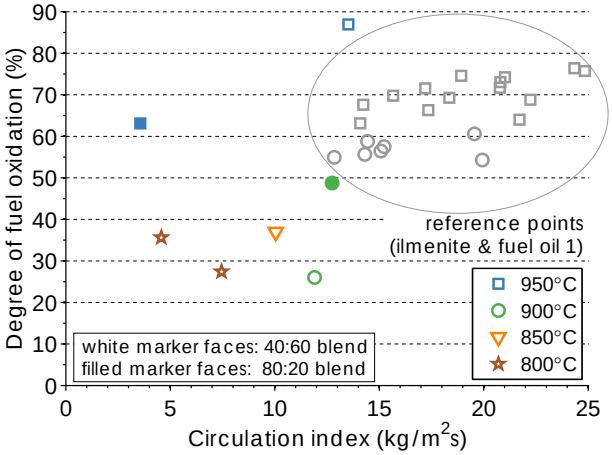

Figure 6: Degree of fuel oxidation, η_{fuel}, with ilmenite oxygen carrier at varied rate of solids circulation, i.e., circulation index, G'_s. Data points are shown for the different fuels used and different fuel-reactor temperatures. The fuel flows correspond to 4.6–5.6 kW_{th} for the 40:60 blend and to 4.5–4.8 kW_{th} for the 80:20 blend. Each data point represents average values for one experimental setting at steady state, which lasted 4–31 min, and 13 min on average. Reference points are taken from [9].

flue gas of the fuel reactor using detector tubes. During that experiment the fuel reactor temperature was between 915°C and 935°C and the degree of fuel oxidation was low, i.e., 50% or below. No SO_2 was detected in the flue gases of the air reactor. In the flue gas of the fuel reactor, the detector-tube measurements indicated quantities of 10000 ppm and 0 ppm of H_2S and SO_2, respectively. The expected amount of sulfur at these conditions is about 13000 ppm. Since most of the sulfur was detected, it can be concluded that most of the sulfur in the gas phase was in the form of H_2S. It is likely that SO_2 was present in the fuel reactor, but that it was almost completely dissolved in condensate on the inside of the gas lines that connect the reactor with the gas conditioning system. H_2S was probably also dissolved, but due to a significantly lower solubility and a larger quantity in the flue gases only a fraction of H_2S was dissolved. The flue gas of the air reactor does not contain steam and no such effects are expected. Earlier publications by different authors, which include experiments and thermodynamic equilibrium calculations, showed that deposition of sulfur on ilmenite oxygen carrier is unlikely, even under highly reducing conditions [23, 24]. In conclusion, no evidence was found that indicates that leakage of sulfur from fuel reactor to air reactor occurs with ilmenite oxygen carrier.

4.2. Calcium Manganite-based Oxygen Carrier

This section consists of three parts. Results attained during 9.6 h of fuel addition are shown and discussed in Sections 4.2.1 and 4.2.2. Changes in the structure of the oxygen carrier due to fluidization under hot conditions, i.e., more than 600°C, cyclic oxidation and reduction as well as the presence of sulfur are shown in Section 4.2.3.

4.2.1. Fuel Conversion

The circulating fluidized-bed system was operated using different amounts of solids inventory. The amount of particles in the system varied during the experiments. This was due to the production of fines as a consequence of particle attrition, as well as elutriation of particles from the system. The latter was due mainly to an imperfectly operating cyclone separator, and, consequently, such elutriation is not expected to be a problem in a large-scale unit. To compensate for the continuous loss of solids inventory, fresh particles were loaded into the system until, eventually, no more fresh particles were available. The circulation index, G'_s, i.e., the gross amount of particles in the riser that are in motion, is shown in Figure 7 at varied superficial gas velocity, u_0, in the riser. It can be seen that the amount of particles used in the system towards the end of the experimental campaign, when no more fresh material was available, i.e., 16–18 kg, was too low to operate the circulating system effectively; the circulation index was low and did not change when the gas velocity was increased.

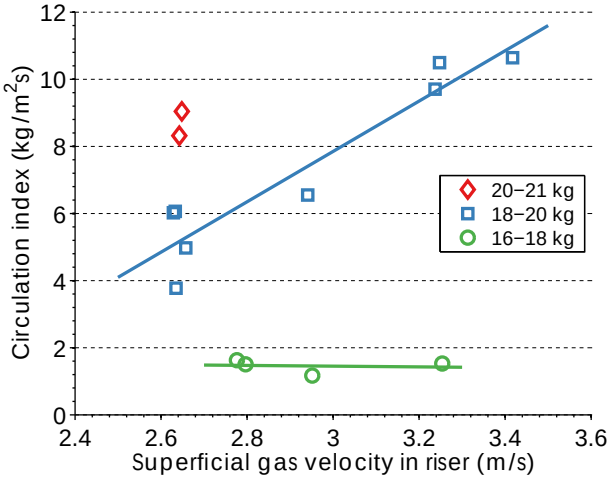

Figure 7: Circulation index, G'_s, with calcium manganite-based oxygen carrier at varied superficial gas velocity, u_0, in the riser and for different amounts of solids inventory. Fitted lines are shown for the solids inventories of 16–18 kg and 18–20 kg.

Figure 8 shows the degree of fuel oxidation, η_{fuel}, i.e., the ratio of oxygen consumed in the air reactor by the stoichiometric amount of oxygen, at varied oxygen-carrier circulation, i.e., circulation index, G'_s, fuel type and fuel input at a temperature of approximately 950°C. For the different experimental settings investigated the oxygen concentration at the outlet of the air reactor varied between 13.5% and 16.5%. The highest degree of fuel oxidation, i.e., 89%, was achieved with fuel oil 1 at a fuel input of 4.4 kW_{th}. With undiluted vacuum residue, the maximum degree of fuel oxidation achieved was 73% at a fuel input of 4.7 kW_{th}, though at a much lower rate of solids circulation as compared to the benchmark with fuel oil 1. Fuel conversion seems to improve with higher rates of solids circulation; but since higher rates of solids circulation were used with lighter fuels (fuel blends), it cannot be said with certainty whether the trend visible in Figure 8a is caused by varying the solids circulation, the fuel type or a combination of both.

Figure 8b shows a clear negative association between fuel input and fuel conversion, which is in accordance with earlier observations [9], and can be explained by one or a combination of the following points. (1) An increased gas flow in the fuel reactor decreases the contact time between oxygen carrier and combustible gas. (2) An increased gas flow might induce gas channels in the fluidized bed, through which combustible gas bypasses the oxygen-carrier bed. (3) The average degree of oxidation of the oxygen carrier, i.e., ω, in the fuel reactor is lowered, which is associated with a reduction in reactivity for conversion of combustible gas [10, 13]. Another trend, which is visible in Figure 8b, is that at similar rates of solids circulation, fuel conversion was higher with fuel oil 1 than with both the 40:60 blend and the 80:20 blend. The reason for this decrease in conversion is not necessarily the change in fuel type. Instead, it could be due to the reduction in the oxygen carrier's reactivity that was observed between oxygen-carrier particles in fresh and used state, see Section 4.2.3 below.

Figures 9a–9d show the different fractions of carbon species in the fuel reactor, γ_{CO_2}, f_{CO}, f_{CH_4} and f_{CHO}, at varied solids circulation, i.e., circulation index, G'_s, fuel type and reactor temperature. The highest level of fuel conversion was achieved with vacuum residue at a fuel input of 5.0 kW_{th} and a temperature of 1000°C in the fuel reactor. Here, the CO_2 yield was 93% and the fractions of CO, CH_4 and $C_xH_yO_z$ were 3.0%, 1.3% and 2.6%, respectively, cf. Equations (5)–(8). Increasing solids circulation clearly improves fuel conversion, i.e., the CO_2 yield increases while the carbon fractions of $C_xH_yO_z$, CH_4 and CO decrease. A distinct difference between the different types of fuel used cannot be seen. Fuel conversion for the experiment at 1000°C, which also was conducted at a higher rate of solids circulation, is clearly better than for the experiments at lower temperature. Unfortunately, there is only one data point available that has a different temperature than the rest, which makes the conclusions from the variation of temperature somewhat uncertain.

The concentration of hydrogen measured was clearly above that of carbon monoxide, which can be attributed to the high hydrogen-to-carbon ratio in the fuel reactor, i.e., H/C. Through the addition of steam for cooling and fluidization, this ratio was between 6.1 and 8.5 during the entire test campaign. The equilibrium concentrations of hydrogen, based on the water-gas shift reaction, were usually 10–20% lower than the measured values. This deviation increased to about 80% when undiluted vacuum residue was used as fuel. Fractions of hydrogen species were not calculated, but the concentrations measured followed the same trends as the carbon fractions of CO, CH_4 and $C_xH_yO_z$ in Figure 9. The highest average concentration of hydrogen was 14.3% and was detected during the addition of 6.2 kW_{th} of fuel oil 1 at a fuel-reactor temperature of 950°C. The lowest average hydrogen concentration was 3.3% and was observed when undiluted vacuum residue was used as fuel at a flow rate that corresponds to 5.0 kW_{th} and a fuel-reactor temperature of 1000°C.

A release of gas-phase oxygen by the oxygen carrier, i.e., a CLOU effect, was clearly seen prior to fuel operation when the fuel reactor was fluidized with steam. At a fuel-reactor temperature of about 900–950°C, after cooling to 4°C, the flue gas contained more than 21% of oxygen, the rest being nitrogen, which was used for fluidization of the loop-seals. The corresponding concentration of oxygen in the fuel reactor was approximately 3%.

4.2.2. Carbon Leakage and Fate of Sulfur

Carbon leakage of the system, $f_{C,AR}$, which is one minus the carbon capture efficiency, was calculated on the basis of the concentration of CO_2 measured in the air reactor. The concentration of CO_2 varied between 600 ppm and 2600 ppm and during eight out of fourteen experiments, it was below 1000 ppm. The corresponding values of the carbon fraction in the air reactor, which are corrected for the atmospheric concentration of CO_2, i.e., 400 ppm, are shown in Figure 10. During most experiments, carbon leakage of fuel carbon to the air reactor was about 1% or below. On three occasions, when vacuum residue and the 80:20 blend were used as fuel, more than 2% of the fuel carbon leaked to the air reactor and would have been lost with respect to carbon capture. The fuel inputs during these experiments were 4.7 kW_{th} and 5.0 kW_{th} with vacuum residue and 4.0 kW_{th} with the 80:20 blend. With these fuels, lower values of carbon leakage were measured at higher fuel inputs. Hence, no clear trend of the carbon fraction in the air reactor at varied circulation, fuel type or fuel input can be observed.

With calcium manganite-based oxygen carrier, an SO_2 analyzer was connected to the air reactor on two occasions, during 38 min and 178 min of fuel operation with 80:20 blend and vacuum residue, respectively. The temperature in the fuel reactor was varied between 920°C and 1010°C and the temperature in the air reactor was 890–1020°C. No SO_2 was detected in these two occasions. Measurements to detect SO_2 and H_2S in the flue gas of the fuel reactor were not performed.

4.2.3. Particle Analysis

Scanning electron microscope (SEM) images of fresh and used calcium manganite-based particles show mostly regular, spherical particles, see Figure 11. The fresh sample contains a significant fraction of small particles and fragments, and the surface porosity varies visibly, see Figure 11a. The particles of the used sample look more homogeneous with regard to size and surface porosity and the surface appears to be less porous in comparison to that of the fresh particles. Almost no donut-shaped particles were seen in any of the samples. SEM images of particle cross-sections revealed that both the fresh and the used oxygen-carrier batches contained particles with large cavities. These types of particles can be formed during the spray-drying procedure at unoptimized conditions. The porosity seen in the cross-sections seems to decrease from fresh to used state, which is in agreement with the observations from the surface images.

Particle size distributions were measured for fresh and used particles by means of sieving and weighing, see Figure 12. Over the course of the campaign, the distribution curve became narrower, i.e., the fractions of particles above 212 µm and below 125 µm decreased, and the form of the distribution curve became more bell-shaped. While the mean particle size remained practically constant, the bulk density increased by nearly 30%,

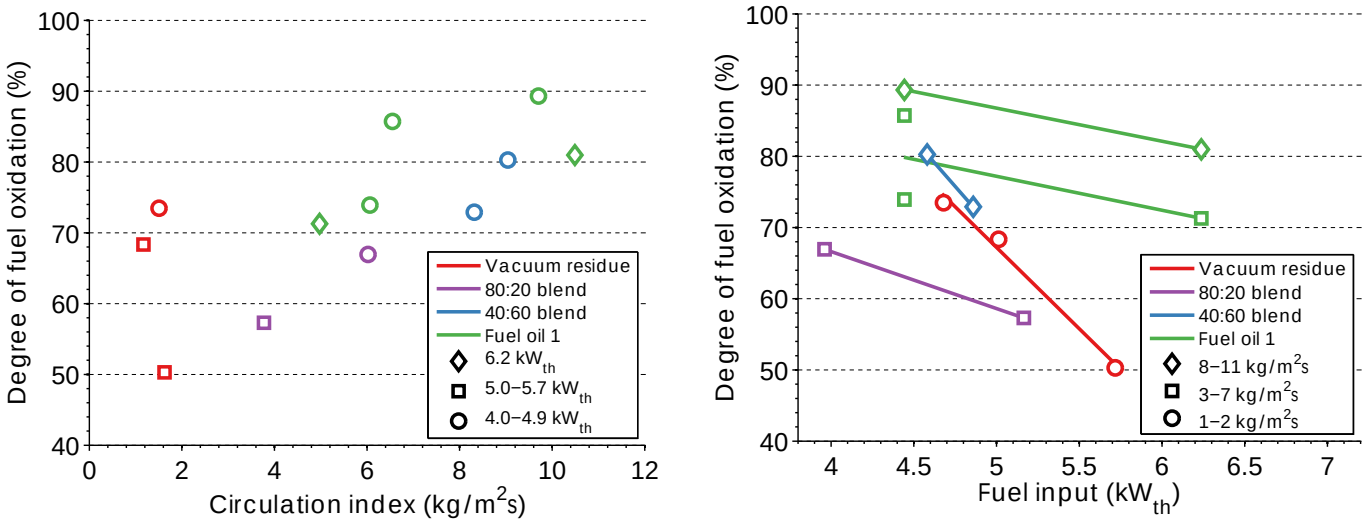

(a) Variation of solids circulation

(b) Variation of fuel input

Figure 8: Degree of fuel oxidation, η_{fuel}, with calcium manganite-based oxygen carrier at **(a)** varied rate of solids circulation, i.e., circulation index, G'_s, and **(b)** varied fuel input. Data points are shown for the different fuels used at a fuel-reactor temperature of approximately 950°C. Colors indicate the fuel type and marker shapes indicate the fuel input in **(a)** and the solids circulation in **(b)**. Fitted lines are shown in **(b)**. Each data point represents average values for one experimental setting at steady state, which lasted 6–25 min, and 16 min on average.

see Table 3. This again confirms a decrease in porosity, and this densification of calcium manganite-based materials was also reported by other authors, though to a smaller extent. Rydén et al. [25] reported an increase in bulk density of 8% over a period of 70 h of experiments in a bench-scale fluidized-bed reactor with continuous oxygen-carrier circulation and natural gas as fuel. Cabello et al. [26] measured the skeletal density during an experimental campaign and observed an increase in density of 5% during 38 h of fuel operation with methane, followed by another increase of 5% during 17 h of fuel operation with sulfurous methane. The resistance to mechanical attrition increased significantly over the course of the experiments, which is indicated by the reduction of the attrition index, see Table 3. A possible explanation of the observed changes could be that the batch of fresh particles consisted of a higher fraction of particles with cavities, which may have a higher propensity to break than more solid particles and, consequently, the fraction of this type of particle was reduced as fragments were elutriated from the system in the cyclone.

Table 3: Characteristics of calcium manganite-based particles in fresh and used state

		Fresh	Used
Harmonic mean particle size, $\overline{x}_{\text{har}}$	(μm)	159	160
Bulk density*	(kg/m^3)	1460	1870
Attrition index†	(wt%/h)	4.1	1.2

*measured on the basis of ISO standard 3923-1

†measured in a customized jet-cup attrition rig [27]

The comparison of fuel conversion against oxygen-carrier conversion for a number of redox cycles conducted in a batch fluidized-bed reactor shows a clear deterioration in reactivity of the oxygen carrier from fresh to used state, see Figure 13. Possible explanations for this decrease in reactivity could be the general susceptibility of calcium manganite-based materials to sulfur poisoning, which has been observed before [11], or the reduction in porosity observed. For an oxygen carrier with a similar composition to the one used here, Arjmand et al. [11] showed that is possible to reverse a sulfur-induced deactivation. Reactivation occurred during a number of redox cycles in a batch fluidized-bed reactor with sulfur-free fuel, at 1000°C and at prolonged inert periods. No such regeneration occurred here during the batch tests conducted with the used, deactivated particles. To see whether sulfur reacted with the particles, an EDX analysis was conducted on the used material.

Particles of the calcium manganite-based oxygen carrier were mounted on an epoxy puck, which was polished, so that the cross-section of the particles could be investigated. Two such samples were produced, one with fresh, heat treated particles and one with particles used during the entire test campaign. EDX measurements were done with a scanning electron microscope (FEI Quanta 200 ESEM FEG) using an acceleration voltage of 20 kV.

A randomly selected area of the sample with used particles, which contained about 70 particle cross-sections, was mapped. The elements Ca, Mn, Ti, S and O were evenly distributed among the particles, with the exception of a few particles that contained less Ca and more Mn, and Mg occurred in some concentrated spots. In about 20% of the cross-sections, the amount of sulfur detected was clearly higher than in the rest of the particles. The atomic fraction of sulfur (out of the elements Ca, Mn, Ti, Mg and S) for one of the particles with a high sulfur concen-

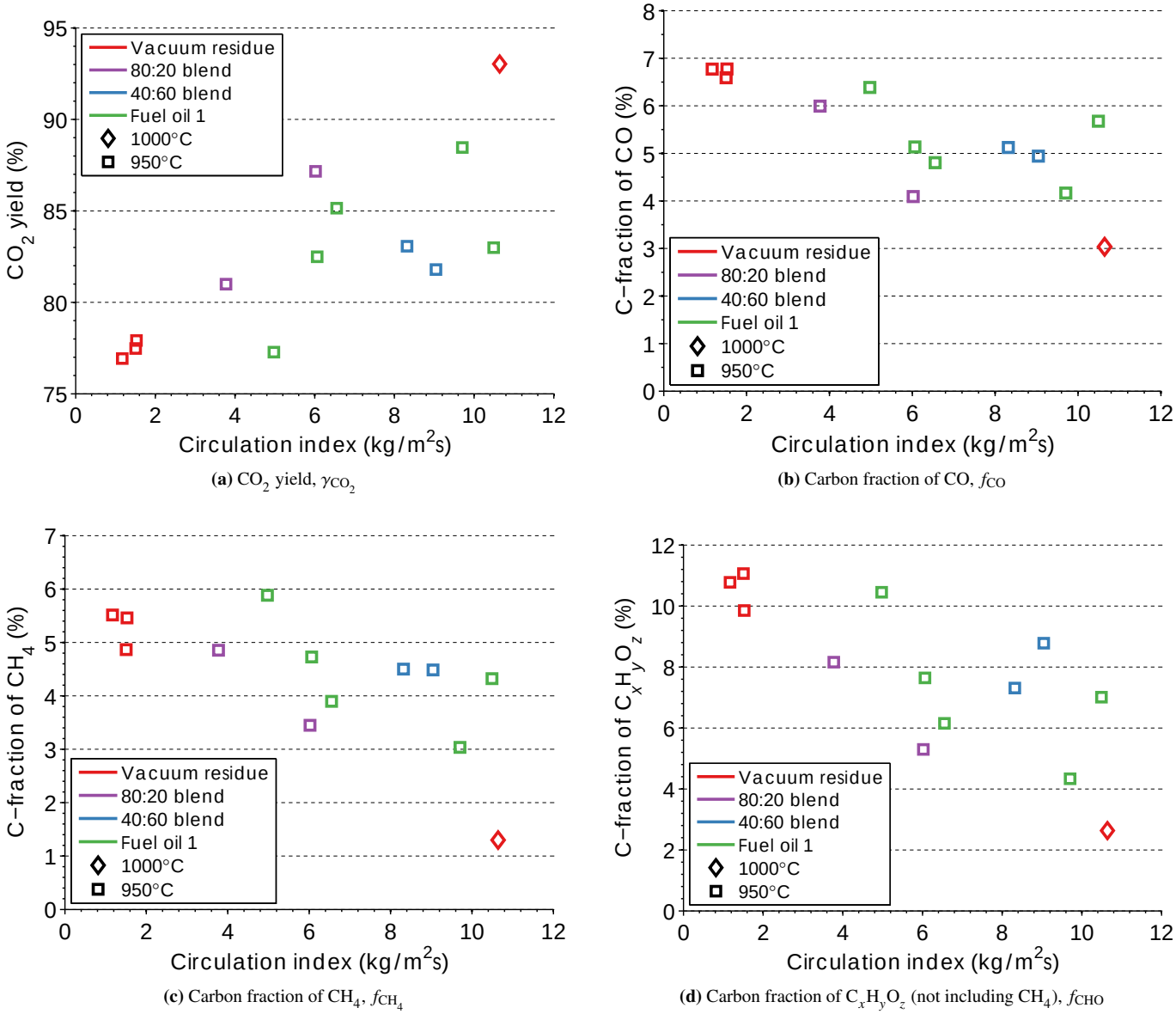

(a) CO_2 yield, γ_{CO_2}

(b) Carbon fraction of CO, f_{CO}

(c) Carbon fraction of CH_4, f_{CH_4}

(d) Carbon fraction of $C_xH_yO_z$ (not including CH_4), f_{CHO}

Figure 9: CO_2 yield, γ_{CO_2}, and carbon fractions, f_i, in the fuel reactor with calcium manganite-based oxygen carrier at varied rate of solids circulation, i.e., circulation index, G'_s, for the different fuels used and different fuel-reactor temperatures. **(a)** CO_2 yield, γ_{CO_2}, **(b)** carbon fraction of CO, f_{CO}, **(c)** carbon fraction of CH_4, f_{CH_4}, and **(d)** carbon fraction of $C_xH_yO_z$ (organic compounds not including CH_4), f_{CHO}. The fuel flows correspond to 4.7–5.0 kW_{th} for vacuum residue, 4.0–5.2 kW_{th} for the 80:20 blend, 4.6–4.9 kW_{th} for the 40:60 blend and 4.4–6.2 kW_{th} for fuel oil 1.

tration was about 0.06. For a particle with low sulfur signal, the atomic fraction of sulfur was less than 0.02. During the whole experimental campaign with calcium manganite-based oxygen carrier, fuel was added for nearly 10 h, which, in total, contained about 100 g of sulfur. If all that sulfur had reacted with 16 kg of bed material, e.g., to form calcium sulfate, an atomic fraction of sulfur of about 0.01–0.02 would have been expected. Hence, it seems likely that a large fraction of the sulfur added reacted with the oxygen carrier. Due to their even distribution, sulfur cannot be clearly associated with calcium or manganese. In the sample of fresh particles, the level of sulfur detected on the particles could not be differentiated from the background level.

Crystalline phases of oxygen-carrier particles were identified using X-ray powder diffraction (Bruker D8 Advance) with CuKα radiation. The diffractograms of fresh and used particles were similar in the analyzed range of $2\theta = 10 \ldots 70°$; the major phase $CaMn_{0.5}Ti_{0.5}O_3$ was identified as well as the minor phases $CaMn_{0.9}Ti_{0.1}O_{2.962}$, $CaMn_2O_4$ and MgO. Crystalline phases of sulfur could not be identified unambiguously.

5. Discussion

Table 4 shows at comparison between fuel conversion with ilmenite and calcium manganite-based oxygen carrier for dif-

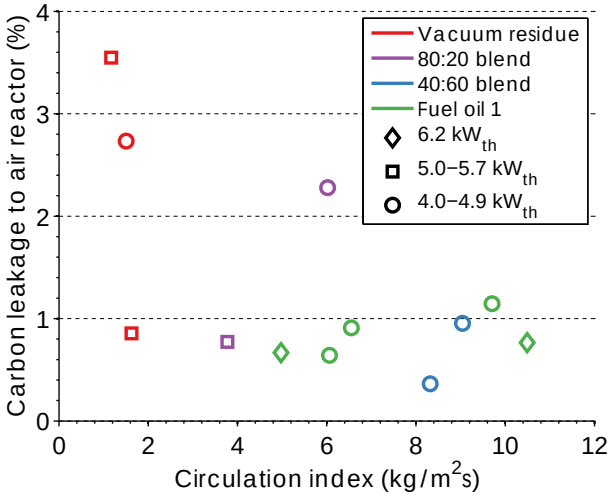

Figure 10: Carbon leakage to the air reactor, $f_{C,AR}$, with calcium manganite-based oxygen carrier at varied rate of solids circulation, i.e., circulation index, G'_s. Data points are shown for the different fuels used at a fuel-reactor temperature of 950°C. The fuel flows correspond to 4.7–5.7 kW_{th} for vacuum residue, 4.0–5.2 kW_{th} for the 80:20 blend, 4.6–4.9 kW_{th} for the 40:60 blend and 4.4–6.2 kW_{th} for fuel oil 1. All values are corrected for the atmospheric concentration of CO_2 during the time of the experiments, i.e., approximately 400 ppm.

ferent fuels (fuel blends). For this comparison, data is shown in chronological order and from experiments where the conditions were as similar as possible. When comparing the values of fuel conversion, it has to be kept in mind that fuel conversion improves at decreased fuel input and at increased solids circulation. Furthermore, the reactivity of the calcium manganite-based oxygen carrier decreased over time, i.e., from fuel oil 1 to vacuum residue. Also, the number of experiments is low and, hence, the uncertainty of each data point is high. With that in mind, it can be seen that the calcium manganite-based oxygen carrier in its initial state, i.e., with fuel oil, exhibited a clearly higher level of fuel conversion than the ilmenite oxygen carrier, even though the fuel input was higher and the level of solids circulation was somewhat lower. Over the course of the experiments with calcium manganite-based oxygen carrier, fuel conversion decreased. This could have been caused by one or a combination of the following: (1) the change of fuel, (2) the deactivation of the oxygen carrier, (3) the decrease in solids circulation. Fuel conversion of the 80:20 blend with ilmenite oxygen carrier is comparable to that of the 80:20 blend and vacuum residue with calcium manganite-based oxygen carrier. The fact that fuel conversion with calcium manganite-based oxygen carrier was initially superior and, over time, approached that of ilmenite oxygen carrier can likely be attributed to the decrease in reactivity, see Figure 13.

The mechanism that caused the deactivation is not fully understood. It was shown (1) that sulfur reacted with the oxygen carrier, (2) that the density of the oxygen carrier had increased and (3) that the surface of the particles seemed to have become less porous. Hallberg et al. [14] showed that the reactivity of a different batch of the calcium manganite-based oxygen carrier used was nearly constant during about 100 h of fuel operation with natural gas. Hence, it seems likely that the decrease in reactivity observed was caused by the sulfur in the fuel. It is unclear to what degree different degrees of sulfur uptake affects the reactivity, and to what extent the material can be regenerated during operation, as was suggested by Arjmand et al. [11]. There, it was seen that captured sulfur was released from the material during extended inert periods, and it was suggested that SO_2 was generated by a reaction of $CaSO_4$ and CaS previously formed. Hence, it could be speculated that SO_2 will be released in regions of low partial pressure of SO_2, i.e., loop-seals and air reactor. It also opens up for the use of a separate regeneration step where sulfur-poisoned oxygen carrier elutriated or extracted from the system is regenerated and transferred back to the chemical-looping system, thus limiting the average degree of deactivation. That said, it is clear that this type of oxygen carrier is most applicable for a desulfurized fuel.

The conversion of fuel in general mainly depends on the following parameters: temperature, fuel flow and oxygen-carrier conversion in the fuel reactor, ω. In the case of oxygen carriers with a perovskite structure, like the calcium manganite-based material used here, the concentration of oxygen at the outlet of the air reactor is added to that list. The oxygen concentration has a direct influence on how much oxygen can be transported to an atmosphere where there is little or no oxygen, i.e., the fuel reactor, as was shown by Rydén et al. [25] and Leonidova et al. [28]. Ideally, in order to show the influence of each of these four parameters, one parameter should have been varied, while holding the others constant. Out of practical reasons this could not be achieved. Here, solids circulation was controlled by varying the air flow to the air reactor. Consequently, solids circulation, air-to-fuel ratio and the concentration of oxygen at the outlet of the air reactor are interdependent and their respective influences are hard to separate.

The greatest challenge during the operation of the circulating fluidized-bed reactor with heavy liquid fuel was the feeding of fuel and blocking of the injection system, respectively. This manifests itself in the low ratio of fuel operation to hot operation (here: above 600°C), i.e., 9.6 h to 94.9 h. The longest periods of fuel feeding were achieved on the last experiment day with vacuum residue. After a period of fuel injection that lasted nearly 1 h, fuel feeding was stopped, restarted and could be continued for another 2 h. This was the first and only time when using 40:60 blend, 80:20 blend or undiluted vacuum residue that fuel injection could be restarted without cleaning or replacing parts of the injection system. For comparison, during an earlier campaign with fuel oil 1 and a similar injection system, fuel feeding could be stopped and restarted without problem and the whole campaign was conducted without the needing of cleaning or replacing parts of the injection system; the longest continuous period of fuel operation was 12.4 h, and a total of 204 h of hot operation yielded 66.6 h of fuel operation [9].

Feeding heavy liquid fuels requires a well-controlled temperature control of the systems for feeding and injection. If the temperature is low, the viscosity is high and the pressure in the fuel system increases. If the temperature falls below the pour

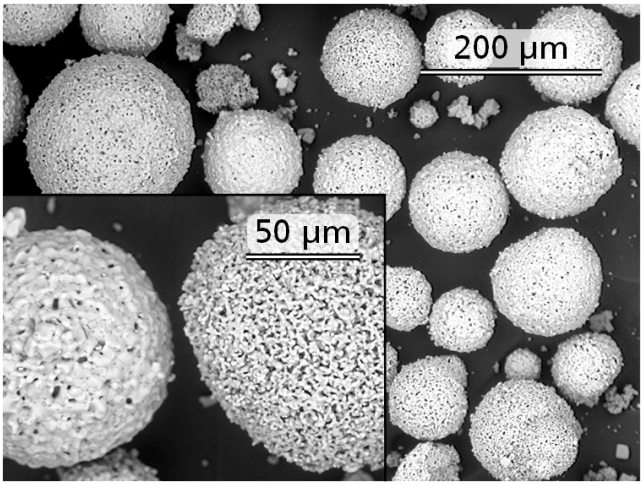

(a) Fresh particles

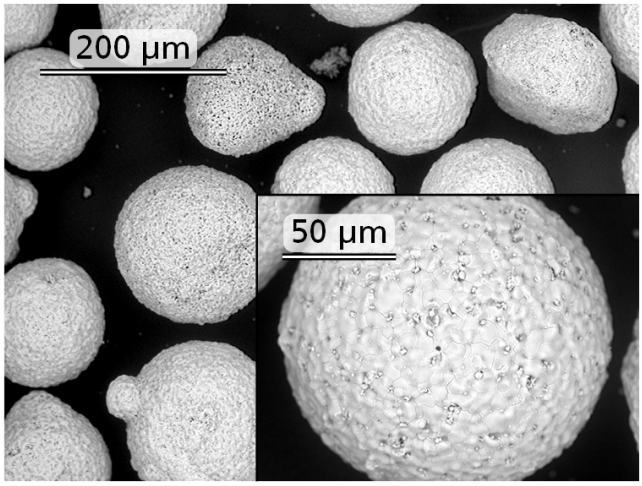

(b) Used particles

Figure 11: Scanning electron microscope (SEM) images of calcium manganite-based particles before and after testing with fuel

Table 4: Comparison of fuel conversion, i.e., degree of fuel oxidation, η_{fuel}, between ilmenite and calcium manganite-based oxygen carriers for different liquid fuels (fuel blends) in the 10 kW unit at similar conditions (temperature, fuel input and solids circulation). The fuels are listed in chronological order.

Order	Fuel (blend)	Oxygen-carrier material	
		Ilmenite	Calcium manganite
1)	Fuel oil 1	4.2–4.3 kW_{th}, 14–16 kg/m^2s, 950°C ⇒ **63–70%**	4.4–6.2 kW_{th}, 8–11 kg/m^2s, 950°C ⇒ **81–89%**
2)	40:60 blend	4.7 kW_{th}, 14 kg/m^2s, 950°C ⇒ **87%**	4.6–4.9 kW_{th}, 8–11 kg/m^2s, 950°C ⇒ **73–80%**
3)	80:20 blend	4.7 kW_{th}, 4 kg/m^2s, 950°C ⇒ **63%**	4.0–5.2 kW_{th}, 3–7 kg/m^2s, 950°C ⇒ **57–67%**
4)	Vacuum residue	not tested	4.7–5.7 kW_{th}, 1–2 kg/m^2s, 950°C ⇒ **50–73%**

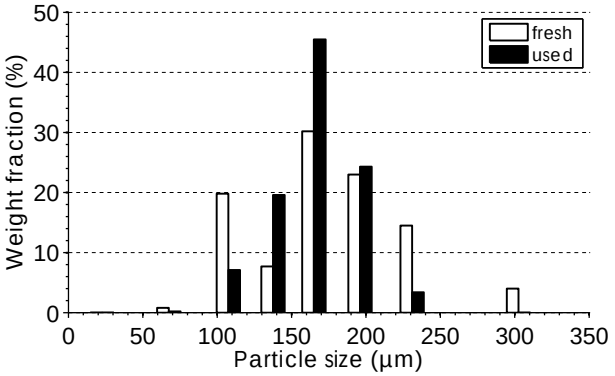

Figure 12: Particle size distribution of calcium manganite-based oxygen carrier before and after testing with different fuels. The particle size distribution was determined through sieving and weighing.

point, cf. Figure 4, the fuel ceases to flow freely. If the temperature of the fuel in the injection system exceeds a critical value, ca. 350°C, the injection system can be blocked because of thermal decomposition and polymerization of the fuel [20]. The fuel temperature in the feeding system can be measured and controlled fairly easily. Monitoring the temperature of the fuel in the injection system, however, which is located in the reactor wall below the surface of a bubbling fluidized-bed, is much more difficult and was not done in this study. Within the injection system, the fuel has the highest temperature in the injection nozzle, where it is fed through an orifice with a diameter of 0.25 mm. While a direct measurement of the fuel temperature here seems virtually impossible, it might be estimated from a temperature measurement at a different point of the injection system. It is expected that monitoring the fuel temperature is easier in systems with higher thermal capacities, larger fuel flows and, consequently, larger injectors.

It is not known if the blocking of the injection system was preceded by a long and slow process of fuel polymerization and carbon deposition or if the process is fast and possibly self-enhancing. This might be important, because if a fraction of fuel carbon were deposited in the injection system, then the composition of the fuel that enters the fluidized bed would change, which, in turn, would affect some of the calculated values. Without correcting the calculations for carbon deposition, the frac-

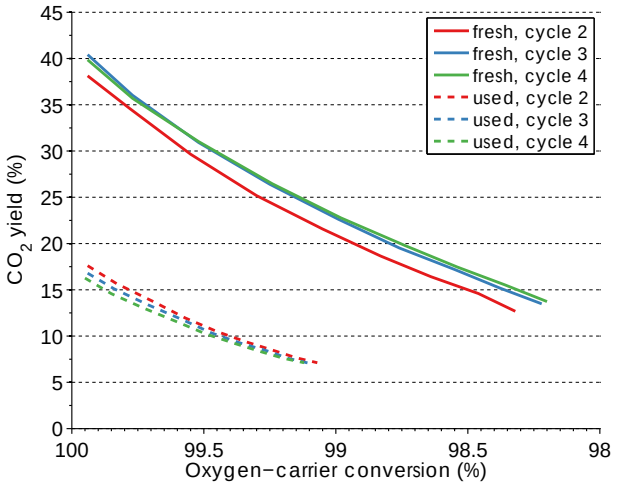

Figure 13: Reactivity comparison of fresh and used calcium manganite-based oxygen carrier with methane as fuel at 950°C. The specific bed mass was 13 kg/MW_{th}. Reactivity is shown as gas conversion, i.e., CO_2 yield, γ_{CO2}, at varied oxygen-carrier conversion, ω, measured for four oxidation and reduction cycles for both fresh and used oxygen carrier. Results from the first cycles are omitted.

tion of carbon that leaks to the air reactor, $f_{C,AR}$, as well as the degree of fuel oxidation, η_{fuel}, could be undervalued. The pressure in the fuel line can be an indicator for how carbon deposition and blocking of the injector occur, abrupt or slow and continuous. With the 40:60 blend and the 80:20 blend, the pressure was stable for 10–20 min, followed by a pressure built-up that lasted 20–60 min and resulted in complete blocking of the injector. With vacuum residue, the pressure fluctuated more and several pressure peaks were observed, and, in contrast to the experiments with blends of vacuum residue and fuel oil 1, pressure peaks were passed without having to stop fuel feeding. After the experiment where vacuum residue was continuously fed for 2 h, and which resulted in blocking of the injector, the injection system and the rest of the reactor system was disassembled. It was found that the fuel injection system was blocked by a cylindrical, solid plug, which was about 5–6 cm long, 12.5 mm in diameter and had a weight of 11.9 g. A sample of this piece was crushed and analyzed with EDX. Only two elements were identified; carbon as the main constituent accompanied by a minor fraction of sulfur. This was the largest and most severe occurrence of a plug in the injection system during the whole campaign and the weight of the plug corresponds to about 1.3 wt% of the total amount of fuel added during the 2 h prior to the blocking. Therefore, it is concluded that the effect of carbon deposition was small and can be neglected. Additionally, at the muzzle of the injection system in the fluidized bed a large, more or less spherical, and rather soft agglomerate had formed, which was about 6 cm in diameter and weighed about 127 g. An SEM/EDX analysis of a crushed sample showed that the agglomerate consists of oxygen-carrier particles, which contain a significant amount of sulfur and virtually no carbon. It is likely that the agglomerate contained some carbon, which was burned during the reoxidation of the oxygen carrier material, prior to cool-down. The analysis of the plug and the agglomerate suggests that (1) fuel fouling in the injection system occurs in the absence of oxygen carrier particles and (2) the presence of sulfur in the fluidized bed might induce an agglomeration of calcium manganite-based oxygen-carrier particles.

Most problems regarding the feeding of heavy liquid fuels are believed to be connected with the injection system and, more precisely, insufficient cooling of the fuel. As discussed above, monitoring the temperature will most likely be easier at a larger scale. The same is probably true for the cooling of fuel, which would need to be improved. A possible solution would be to add a closed cooling circuit into the wall of the existing injection system to reduce heat transfer to the injection nozzle.

Carbon leakage from fuel reactor to air reactor occurred with both oxygen carrier materials as well as with all fuels investigated. The mechanism that causes carbon leakage cannot be clearly distinguished. Possible mechanisms for carbon leakage are gas leakage, carbon deposition on oxygen-carrier particles and soot formation in the fuel-reactor bed. The latter two mechanisms involve formation of solid carbon in the fuel reactor, which follows the circulation of oxygen-carrier particles into the air reactor. In the 10 kW reactor used, neither gas leakage nor carbon formation occurred during more than 1000 h of fuel operation with natural gas [29, 30]. Hence, it is unlikely that gas leakage should occur when employing liquid fuels. In this study, carbon deposition occurred regularly in the injection system, even though it should have been suppressed by the high amount of steam. Hence, it seems possible that soot is formed in the particle bed close to the injector. Soot particles, however, are small and, therefore, would be elutriated from the particle bed by the flow of gas or, alternatively, gasified by the steam present in the fuel reactor. Carbon formation on the oxygen-carrier particles should be thermodynamically impossible, inhibited by the high steam content in the fuel reactor and, in case of the calcium manganese-based material, the fact that oxygen is released from the particles. Carbon deposition, which is autocatalytic, could occur locally, i.e., in regions where either mixing is poor or where the oxygen carrier is highly reduced, e.g., close to the injection system. Carbon deposition on the oxygen carrier particles and subsequent transport to the air reactor seems to be the most likely mechanism for carbon leakage.

6. Summary and Conclusions

In this study, chemical-looping combustion of a heavy liquid fuel was conducted using a continuous CLC unit. A fuel reactor with an in-situ fuel-injection system for heavy liquid hydrocarbon fuel, i.e., vacuum residue, was designed and constructed for a chemical-looping reactor system with the nominal fuel input of 10 kW_{th}. In this system, the gas velocities in both riser and gas-distributor nozzles are comparable to those of an industrial circulating fluidized-bed boiler. Ilmenite and a calcium manganite-based oxygen carrier were used for reference and performance experiments, respectively, and different fuels including a vacuum residue, a fuel oil and blends of those were tested.

During the reference experiments, the degree of fuel oxidation was 25–87% and usually less than 2.5% of the fuel carbon leaked into the air reactor. In the fuel reactor, fuel sulfur was converted mostly to H_2S and possibly some SO_2 and no evidence was found that sulfur was transported to the air reactor. The variability in the measured data was high, likely due to difficulties in maintaining steady-state.

Experiments with successful injection of undiluted vacuum residue were performed using a calcium manganite-based material, which has a perovskite structure and can release gas-phase oxygen in the fuel reactor. The latter characteristic can be highly beneficial for the conversion of liquid or solid fuels. Fuel addition took place during almost 10 h and the oxygen carrier was fluidized at hot conditions for more than 90 h. Fuel-reactor temperatures of 950°C and 1000°C were tested at varied circulation of solids, air-to-fuel ratio, fuel type and fuel input. The fuel input was between 4.0 kW_{th} and 6.2 kW_{th}, which corresponds to a specific fuel-reactor bed mass of about 1300–2000 kg/MW_{th}, which is high. Fuel oxidation increased with higher temperatures, lower fuel input, higher air-to-fuel ratio and higher circulation rates of oxygen carrier. A distinct dependence of fuel conversion on the fuel type used could not be seen. At a fuel-reactor temperature of 1000°C and an input of vacuum residue that corresponds to 5.0 kW_{th}, about 93% of all carbon leaving the fuel reactor was in the form of CO_2. Carbon leakage to the air reactor was very low and usually below 1%. The reactivity of the oxygen carrier decreased over time, which is probably an effect of sulfur poisoning. Despite that, no sulfur was detected in the flue gas of the air reactor.

With fuel oil 1, fresh calcium manganite-based oxygen carrier exhibited clearly higher degrees of fuel oxidation than activated ilmenite. With blends of vacuum residue and fuel oil 1, used, i.e., deactivated, calcium manganite-based oxygen carrier exhibited degrees of fuel oxidation similar to those achieved with activated ilmenite.

The following conclusions can be drawn:

- Successful injection of different heavy liquid fuel blends was achieved even though problems with recurrent blocking of the injection system could not be overcome.
- The use of different fuel types did not have a visible effect on fuel conversion or carbon leakage, i.e., vacuum residue, fuel oil 1 and blends of the two exhibited a similar behavior. However, the sulfur present in the vacuum residue can clearly have a negative effect on the reactivity of the calcium manganite-based oxygen carrier.
- Stable operation was achieved, despite the short injection times, i.e., 38–178 min.
- The integrity of the calcium manganite-based oxygen carrier was high and no noteworthy problems, such as high formation of fines, agglomeration of bed material or defluidization, were encountered.
- With calcium manganite-based oxygen carrier, most of the fuel sulfur was retained in the bed. It is likely that the Ca in the oxygen carrier forms $CaSO_4$ or CaS.
- The calcium manganite-based oxygen carrier exhibited a decrease in reactivity, likely due to sulfur poisoning.

Nomenclature

$\mathrm{d}h_{\mathrm{exit}}$	(m)	height difference of pressure drop $\mathrm{d}p_{\mathrm{exit}}$
$\mathrm{d}p_{\mathrm{exit}}$	(Pa)	pressure drop at the exit of the riser
$f_{\mathrm{C,AR}}$	(mol/mol)	carbon fraction of fuel carbon leaking to air reactor, Eq. (4)
$f_{\mathrm{CH_4}}$	(mol/mol)	carbon fraction of CH_4 in fuel reactor, Eq. (7)
f_{CHO}	(mol/mol)	carbon fraction of $C_xH_yO_z$, not including CH_4, in fuel reactor, Eq. (8)
f_{CO}	(mol/mol)	carbon fraction of CO in fuel reactor, Eq. (6)
g	(m/s^2)	gravitational acceleration constant = 9.81 m/s^2
G_{s}	(kg/m^2s)	mass flux of oxygen carrier, Eq. (1)
G'_{s}	(kg/m^2s)	circulation index (gross mass-flux of oxygen carrier), Eq. (2)
m_{OC}	(kg)	actual mass of oxygen carrier
$m_{\mathrm{OC,ox}}$	(kg)	mass of oxygen carrier in the most oxidized state
$\dot{n}_{\mathrm{C,fuel}}$	(mol/s)	molar flow of elemental carbon in the fuel added
$\dot{n}_{\mathrm{CO_2,AR,out}}$	(mol/s)	molar flow of carbon dioxide leaving the air reactor compensated for atmospheric CO_2 concentration ($\approx$ 400 ppm)
$\dot{n}_{\mathrm{O_2,AR,in}}$	(mol/s)	molar flow of oxygen entering the air reactor
$\dot{n}_{\mathrm{O_2,AR,out}}$	(mol/s)	molar flow of oxygen leaving the air reactor
$\dot{n}_{\mathrm{O_2,stoich}}$	(mol/s)	stoichiometric molar flow of oxygen for combustion of fuel
u_0	(m/s)	superficial gas velocity
u_{t}	(m/s)	terminal velocity based on average particle size
$x_{10,90}$	(μm)	distribution points in the particle size distribution of a material based on weight, i.e., 10 wt% of all particles are smaller than x_{10} and 90 wt% of all particles are smaller than x_{90}
$\overline{x}_{\mathrm{har}}$	(μm)	harmonic mean particle size based on weight
x_i	(mol/mol)	concentration of species i

γ_{CO_2}	(mol/mol)	CO_2 yield, Eqs. (5) & (10)
Δh	(m)	height difference of middle section of the riser = 0.678 m
Δp	(Pa)	pressure drop measured in middle section of the riser
η_{fuel}	(mol/mol)	degree of fuel oxidation, Eq. (3)
ρ_{exit}	(kg/m^3)	(two-phase) bed density at the exit of the riser
ω	(kg/kg)	degree of mass-based conversion, Eq. (9)
40:60 blend		fuel blend of 40 wt% vacuum residue in fuel oil 1
80:20 blend		fuel blend of 80 wt% vacuum residue in fuel oil 1
AR		air reactor
GC		gas chromatograph
FID		flame-ionization detector
FR		fuel reactor
SEM		scanning electron microscope/microscopy
XRD		X-ray powder diffraction/diffractometry

Acknowledgements

The study is carried out under the project "Chemical-looping with liquid hydrocarbon fuels" financed by Saudi Aramco. Special thanks to Malin Hanning and Peter Hallberg for both company and helping hands during the experiments, to Jessica Bohwalli and Sebastian Sundqvist for helping with SEM/EDX measurements and to Martin Keller for expert help with XRD and for conducting the reactivity analysis.

References

[1] United Nations Framework Convention on Climate Change, Decisions adopted by the Conference of the Parties, in: Report of the Conference of the Parties on its twenty-first session, held in Paris from 30 November to 11 December 2015, FCCC/CP/2015/10/Add.1, Paris, France, 2015.

[2] European Council, 2030 Climate and Energy Policy Framework, in: Conclusions adopted by the European Council (23-24 October 2014), EUCO 169/14, Brussels, Belgium, 2014.

[3] J. Adánez, A. Abad, F. García-Labiano, P. Gayán, L. F. de Diego, Progress in chemical-looping combustion and reforming technologies, Progress in Energy and Combustion Science 38 (2) (2012) 215–282.

[4] A. Lyngfelt, Chemical-looping combustion of solid fuels – Status of development, Applied Energy 113 (2014) 1869–1873.

[5] A. Nandy, C. Loha, S. Gu, P. Sarkar, M. Karmakar, P. Chatterjee, Present status and overview of Chemical Looping Combustion technology, Renewable and Sustainable Energy Reviews 59 (2016) 597–619.

[6] M. Rydén, Chemical looping combustion of liquid fuels, chap. 13, Woodhead Publishing Series in Energy, Woodhead Publishing, 287 – 298, 2015.

[7] A. Lyngfelt, B. Leckner, T. Mattisson, A fluidized-bed combustion process with inherent CO_2 separation; application of chemical-looping combustion, Chemical Engineering Science 56 (2001) 3101–3113.

[8] M. Källén, M. Rydén, C. Dueso, T. Mattisson, A. Lyngfelt, $CaMn_{0.9}Mg_{0.1}O_{3-\delta}$ as oxygen carrier in a gas-fired 10 kW_{th} chemical-looping combustion unit, Industrial and Engineering Chemistry Research 52 (21) (2013) 6923–6932.

[9] P. Moldenhauer, M. Rydén, T. Mattisson, A. Hoteit, A. Jamal, A. Lyngfelt, Chemical-Looping Combustion with Fuel Oil in a 10 kW Pilot Plant, Energy & Fuels 28 (9) (2014) 5978–5987.

[10] P. Hallberg, M. Källén, D. Jing, F. Snikjers, J. van Noyen, M. Rydén, A. Lyngfelt, Experimental investigation of $CaMnO_{3-\delta}$ based oxygen carriers used in continuous Chemical-Looping Combustion, International Journal of Chemical Engineering 2014, no. 412517.

[11] M. Arjmand, R. Kooiman, M. Rydén, H. Leion, T. Mattisson, A. Lyngfelt, Sulfur tolerance of $Ca_xMn_{1-y}M_yO_{3-\delta}$ (M = Mg, Ti) perovskite-type oxygen carriers in chemical-looping with oxygen uncoupling (CLOU), Energy & Fuels 28 (2) (2014) 1312–1324.

[12] M. Keller, H. Leion, T. Mattisson, H. Thunman, Investigation of natural and synthetic bed materials for their utilization in chemical looping reforming for tar elimination in biomass-derived gasification gas, Energy & Fuels 28 (6) (2014) 3833–3840.

[13] D. Jing, M. Jacobs, P. Hallberg, A. Lyngfelt, T. Mattisson, Development of $CaMn_{0.775}Mg_{0.1}Ti_{0.125}O_{3-\delta}$ oxygen carriers produced from different Mn and Ti sources, Materials and Design 89 (2016) 527–542.

[14] P. Hallberg, M. Hanning, M. Rydén, T. Mattisson, A. Lyngfelt, Investigation of a Calcium Manganite as Oxygen Carrier during 99 h of Operation of Chemical-Looping Combustion in a 10 kW_{th} Reactor Unit, International Journal of Greenhouse Gas Control; accepted for publication.

[15] K. Mayer, S. Penthor, T. Pröll, H. Hofbauer, The different demands of oxygen carriers on the reactor system of a CLC plant - Results of oxygen carrier testing in a 120 kW_{th} pilot plant, Applied Energy 157 (2015) 323–329.

[16] T. Olsen, An Oil Refinery Walk-Through, Chemical Engineering Progress 110 (5) (2014) 34–40.

[17] American Bureau of Shipping, Notes on Heavy Fuel Oil, Technical report, American Bureau of Shipping, Houston, TX, USA, 1984.

[18] W. Shu, A Viscosity Correlation for Mixtures of Heavy Oil, Bitumen, and Petroleum Fractions, Society of Petroleum Engineers Journal 24 (3) (1984) 277–282.

[19] Swedish Standards Institute, SS 155410:2011: Fuel oils - Requirements, Swedish Standards Institute, Stockholm, Sweden, STD-81647, 2011.

[20] A. Watkinson, Critical review of organic fluid fouling, technical report ANL/CNSV-TM-208, Argonne National Laboratory, Argonne, IL, USA, 1988.

[21] F. Johnsson, A. Vrager, B. Leckner, Solids flow pattern in the exit region of a CFB-furnace — influence of exit geometry, in: Proceedings of the 15th International Conference on Fluidized Bed Combustion, Savannah, GA, USA, 1999.

[22] D. Kunii, O. Levenspiel, Fluidization engineering, Butterworth–Heinemann, Boston, MA, USA, 2nd edn., 1991.

[23] P. Moldenhauer, M. Rydén, T. Mattisson, M. Younes, A. Lyngfelt, The use of ilmenite as oxygen carrier with kerosene in a 300 W CLC laboratory reactor with continuous circulation, Applied Energy 113 (2014) 1846–1854.

[24] M. Keller, M. Arjmand, H. Leion, T. Mattisson, Interaction of mineral matter of coal with oxygen carriers in chemical-looping combustion (CLC), Chemical Engineering Research and Design 92 (9) (2014) 1753–1770.

[25] M. Rydén, A. Lyngfelt, T. Mattisson, $CaMn_{0.875}Ti_{0.125}O_3$ as oxygen carrier for chemical-looping combustion with oxygen uncoupling (CLOU)—Experiments in a continuously operating fluidized-bed reactor system, International Journal of Greenhouse Gas Control 5 (2) (2011) 356–366.

[26] A. Cabello, A. Abad, P. Gayán, L. De Diego, F. García-Labiano, J. Adánez, Effect of operating conditions and H_2S presence on the performance of $CaMg_{0.1}Mn_{0.9}O_{3-\delta}$ perovskite material in chemical looping combustion (CLC), Energy & Fuels 28 (2) (2014) 1262–1274.

[27] M. Rydén, P. Moldenhauer, S. Lindqvist, T. Mattisson, A. Lyngfelt, Measuring attrition resistance of oxygen carrier particles for chemical looping combustion with a customized jet cup, Powder Technology 256 (2014) 75–86.

[28] E. Leonidova, I. Leonidov, M. Patrakeev, V. Kozhevnikov, Oxygen non-stoichiometry, high-temperature properties, and phase diagram of $CaMnO_{3-\delta}$, Journal of Solid State Electrochemistry 15 (5) (2011) 1071–1075.

[29] C. Linderholm, A. Abad, T. Mattisson, A. Lyngfelt, 160 h of chemical-looping combustion in a 10 kW reactor system with a NiO-based oxygen carrier, International Journal of Greenhouse Gas Control 2 (4) (2008) 520–530.

[30] C. Linderholm, T. Mattisson, A. Lyngfelt, Long-term integrity testing of spray-dried particles in a 10-kW chemical-looping combustor using nat-

ural gas as fuel, Fuel 88 (11) (2009) 2083–2096.